August 2007 Volume 3 Issue 2

Trade Science Inc.

Materials Science

An Indian Journal

Full Paper

MSAIJ, 3(2), 2007 [82-88]

Optical Investigation Of The Thermal Annealing Dependence Of Selenium Films

A.A. Joraid

Department of Physics, Taibah University, Madinah, (SAUDI ARABIA)

Tel: 00966-48226462; fax: 00966-48233727

E-mail : aaljoraid@taibahu.edu.sa

Received: 12th April, 2007 ; Accepted: 17th April, 2007

ABSTRACT

Two types of Se films were deposited on glass substrates by the thermal evaporation technique. Thin films of thickness 393 and 652 nm and thick films of thickness 2642 nm were deposited. A range of annealing temperatures from 323 up to 373 K was used for the films which had a thickness of 652 nm. X-ray diffraction (XRD) investigations indicate the development of crystalline phases as the annealing temperature reaches a transition temperature of 347 K. The effects of annealing were revealed by studying the morphology of the samples using scanning electron microscopy (SEM) and atomic force microscopy (AFM). The refractive index, *n*, was found to be dependent on the annealing temperature and film thickness. The mechanism of the optical absorption follows both the direct and indirect transitions. The indirect, E_{gi}, and direct, E_{gd}, optical band gaps were found to be nearly constant with increasing annealing temperature, followed by a sharp decrease after the transition temperature of 347 K. Both E_{gi} and E_{gd} were found to be film thickness dependent.

KEYWORDS

Selenium;
Thin films;
Optical properties;
SEM;
AFM.

INTRODUCTION

During the past twenty years amorphous semiconductors have become increasingly important because of their significance applications in modern technology. The technological aspects of these materials can be roughly divided into classes[1]: (1) hydrogenated amorphous silicon type alloys, whose applications include solar cells, thin film transistors, image scanners, electrophotography, optical recording and sensors; (2) amorphous chalcogenides, whose applications include such as switching, electrophotography and memory devices. Recently, new optimistic applications of chalcogenides materials have occurred in the field of infrared spectroscopy, laser and fiber techniques[2,3]. One reason for this increase in interest lies in the fact that some amorphous substances show certain unusual switching properties,

which could be important in modern technology applications.

Thin films amorphous selenium are now being introduce in digital radiology[4]. Selenium and its compounds continue to be a subject of great interest. Selenium exists in one of four structures. The most stable crystal form is trigonal (hexagonal) selenium, which consists of helical Se_n chains. Both monoclinic α and β selenium consist of Se_8 rings. Se atoms in the same chain or ring are bonded with a covalent bond and the chains or rings are bonded to each other by van der Waals' forces. The last form of selenium is an amorphous one, consisting of a mixture of chains and rings depending on the method of its preparation[5].

In the present work, the effect of thermal annealing on the optical properties of Se films have been studied in the wavelength range 190-2500 nm. The optical properties have been correlated with scanning electron microscopy (SEM) and atomic force microscopy (AFM) examinations.

EXPERIMENTAL

Selenium powder used in this study was obtained from Sigma Aldrich Co., with purity of 99.99%. The films were deposited onto rectangular, optically flat, standard microscope slide substrates of thickness 1 mm at room temperature. The slide substrates were carefully cleaned ultrasonically in acetone and then rinsed with deionized water. The evaporation was carried out by resistive heating of the desired weight of approximately 20mg of the material from a tungsten boat. The boat was heated by passing a high current(100A) under a base vacuum of 7.5×10^{-8} pa during the deposition process. The substrate base was kept under mechanical rotation to maintain the homogeneity of all the films.

The transmittance, T(λ), and reflectance, R(λ), spectra of the films were measured at normal incidence and at an incident angle of 5^0, respectively. The measurements were acquired in air and at room temperature in the spectral range of 190–2500 nm by using a computer-aided double-beam spectrophotometer (Shimadzu 3150 UV-VIS-NIR) with a resolution of 0.1 nm.

The Se structure was examined using a Shimadzu XRD-6000 X-ray diffractometer using cuk_α radiation (λ=1.5418Å). The X-ray tube voltage and current were 40 kV and 30 mA, respectively.

The condition of the surface microstructure was observed by AFM (Veeco CP-II) in contact mode with Si tips at a scan rate of 1 Hz. The surface microstructure was also revealed by SEM (Shimadzu Superscan SSX-550).

The film thicknesses were deduced from SEM and AFM measurements on the edge of the tilted film and also calculated with a film thickness program (Shimadzu UV-2501PC Film Thickness). Three groups of films were deposited: thin films and thick films having a thickness of approximately 393, 652, and 2642 nm. Temperature-dependent annealing (T_a) at 323, 343, 347, 350, 353, 363, 373, 383, and 403 K for 15 min under a base vacuum of $2\ x10^{-8}$pa was used for the films.

RESULTS AND DISCUSSION

Structural properties

The XRD patterns of the as-deposited Se films and those obtained after heating at different annealing temperatures, T_a, are shown in figure 1.

The deposited film was amorphous. Annealing at various temperature, T_a , increased the sharpness of the line, indicating grain growth. The patterns shown in figure 1 corroborate well with the results given by JCPDS 06-0362. Two main peaks are observed at $2\theta=23.75^0$(100) and 29.77^0(101) indicating a hexagonal structure. The individual crystallite grain size was determined using Scherrer's relation and was found to be in the range 17.2-20.1 nm for

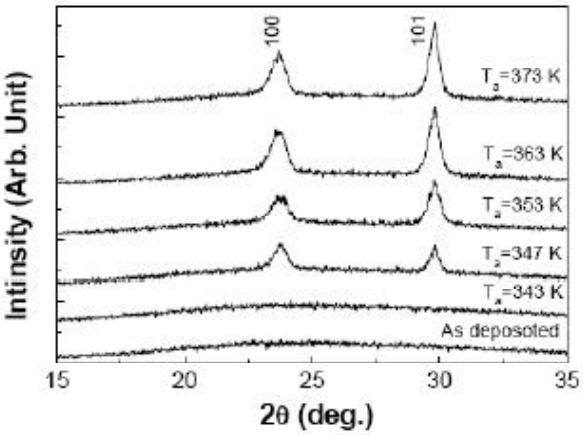

Figure 1: The XRD patterns of the as-deposited film and of the annealed films at different annealing temperatures, T_a

Full Paper

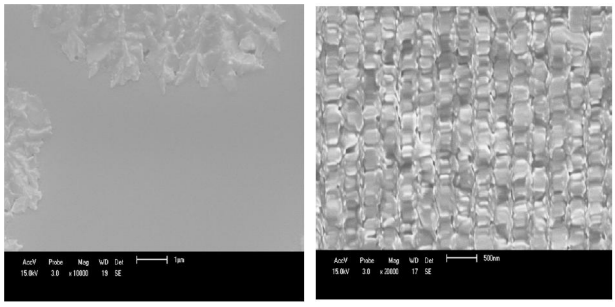

(a) as-deposited (b) annealed at 403 K

Figure 2: SEM patterns of the surface of Se thin films

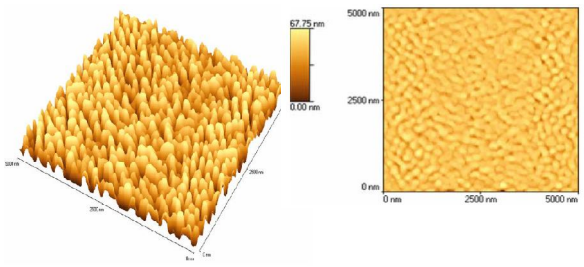

(a) (b)

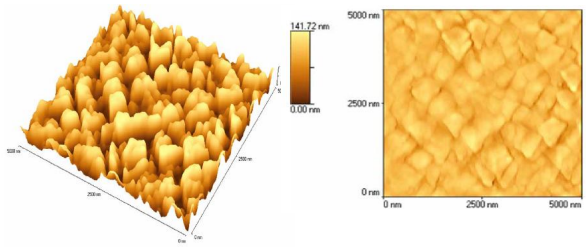

(c) (d)

Figure 3: 5μm×5μm AFM patterns of the surface of Se thin films: (a) 3-D as-deposited, (b) 2-D as-deposited, (c) 3-D annealed at 403 K, (d) 2-D annealed at 403 K

temperatures from 347 to 403 K. The condition of the surface microstructure for Se thin films has been studied by Joraid[6] with SEM and AFM techniques.

The micrograph of the as-deposited film shown in figure 2a reveals the formation of a heterogeneous cluster in the glassy matrix. Normally, Se crystallization proceeds via the formation of spherulites having a lamellar structure, with the width of the lamellae much less than the length of the extended Se chain[6]. However, figure 2b shows homogeneous growth resulting from the lamellae formed after isothermal annealing at Ta=403K.

In addition, the surface morphology of the as-deposited and annealed films were observed by AFM. Figures 3a-d show a three- and two-dimensional view of the amorphous and crystalline Se films. The image in figure 3a shows that the film is made up of a fairly smooth surface with very minute grains which are about 40.6nm in size and have a low roughness of around 1.91nm. The individual grains are separated and are clearly visible. Figure 3c shows the image of a crystalline Se film after annealing at 403 K. The grain size dramatically increased and gave a value of 322.6 nm; the roughness also increased to a value of 11.87 nm. Compared with the earlier amorphous picture, the grains here seem to be in good contact. The increased surface roughness was ascribed to major grain growth; this behavior has been observed for other chalcogenide glasses[7]. Figure 4 shows the individual crystallite grain size obtained by XRD for temperatures ranging from 347 to 403 K. This figure also shows the variation of the grain size obtained by AFM for the as-deposited and annealed films.

Optical studies

Figures 5 and 6 show the spectral behavior in the range from 500 to 2500nm for the transmittance, and the reflectance, respectively. The data obtained were for the as-deposited film and for films annealed at various temperatures (323-373 K) with a thickness of about 652 nm. Figure 7 shows the transmittance and reflectance for the as-deposited thick film with a thickness of about 2642 nm. It is clear from figure 5 that for the as-deposited and annealed films at 323, 333, and 343 K the spectra are identical and

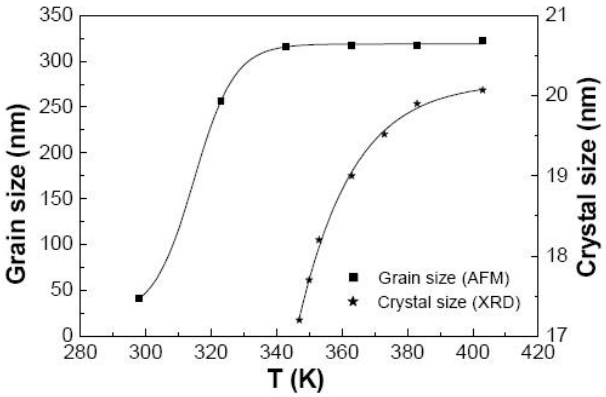

Figure 4: The variation of crystallite grain size obtained by XRD and the grain size obtained by AFM as a function of annealing temperature

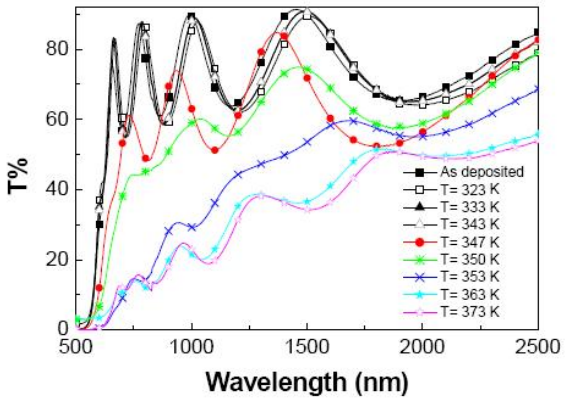

Figure 5: The spectral behavior in the range from 500 to 2500 nm of the transmittance, T(λ), for the as-deposited and annealed Se thin films

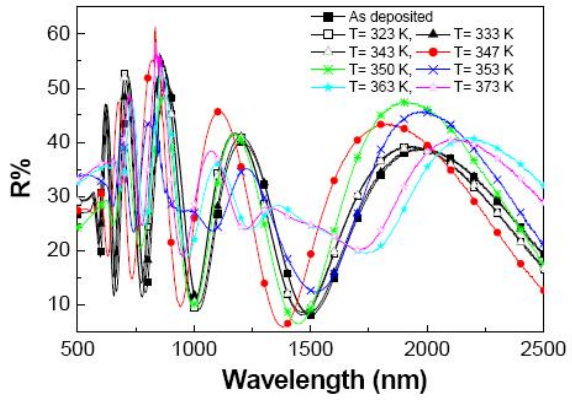

Figure 6: The spectral behavior in the range from 500 to 2500nm of the reflectance, R(λ),for the as-deposited and annealed Se thin films

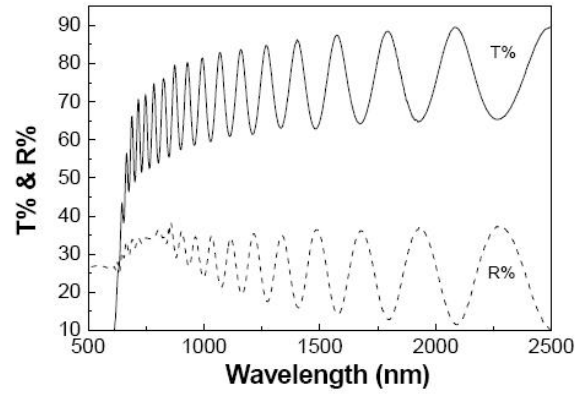

Figure 7: The spectral behavior in the range from 500 to 2500 nm of the transmittance, T(λ), and the reflectance, R(λ), for the as-deposited Se thick films

only a very slight effect was observed. On the other hand, thermal annealing at decreased the transmittance of the as-deposited film and reduced the oscillations of the interference fringes; this reduction becomes stronger as the annealing temperature increases.The refractive indices, η, were computed using an optical characterization method based mainly on the ideas of Swanepoel, utilizing the upper and lower envelopes of the spectrum[8,10]; this is based on a proposal by Manifacier et al.[11]. The refractive index, η, at the transparent region can be calculated from the following equation:

$$\eta = \left(H + \left(H^2 - S^2 \right)^{1/2} \right)^{1/2} \quad (1)$$

Where

$$H = \frac{4S^2}{(S^2+1)T_\alpha^2} - \frac{(S^2+1)}{2} \quad (2)$$

where S is the refractive index of the substrate and T_α is the geometric mean of T_{max} and T_{min}(T_{min} and T_{max}) and are the transmission maximum and the corresponding minimum at certain wavelength). i.e.

$$T_a = (T_{max} T_{max})^{\frac{1}{2}} \quad (3)$$

The values of the refractive indexes of Se at different temperatures, calculated from the transmission spectra, are shown in figure 8. In general it can be seen that the refractive index has a tendency to increase with an increase in the annealing temperature, which may be due to the change in transmittance. An extraordinary increase in the refractive index was recognized as the temperature reached 347 K. This could be ascribed to the change from the amorphous to the crystalline state, as clear from the XRD pattern and AFM results (figures 1 and 4, respectively). This means that the heat treatment changes the optical properties of the film through structural transformation.

The effect of the film thickness on the refractive index is shown in figure 9, where the refractive index is drawn against the wavelength for the three kinds of films (393, 652, and 2642 nm thicknesses).

At the fundamental absorption edge in most amorphous semiconductors the absorption coefficient, α , can be calculated using the expression[12,14]:

$$T = \frac{(1-R)^2 e^{-\alpha d}}{1 - R^2 e^{-2\alpha d}} \approx (1-R)^2 e^{-\alpha d} \quad (4)$$

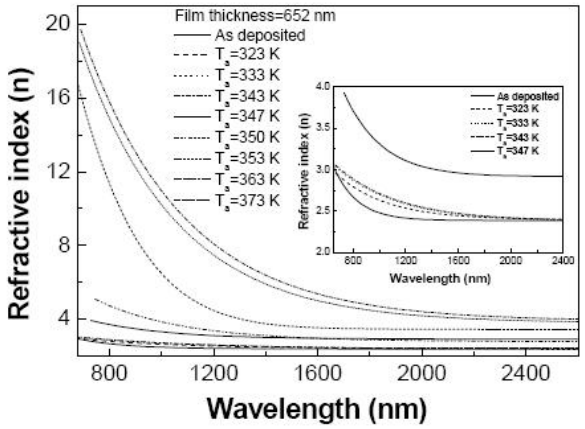

Figure 8: The spectral distribution of the refractive index, $\eta(\lambda)$for the Se thin films, both as-deposited and as obtained at different annealing temperatures

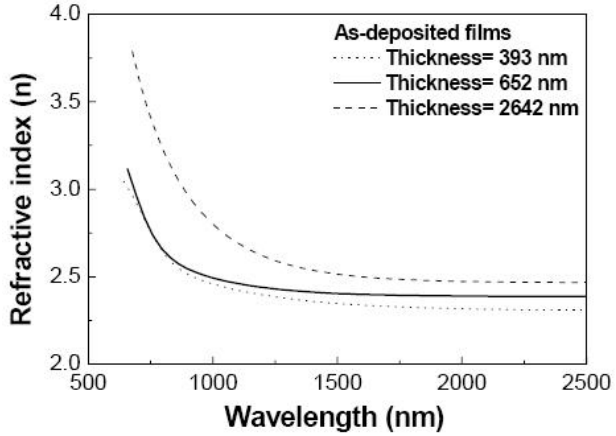

Figure 9: The effect of the film thickness on the refractive index

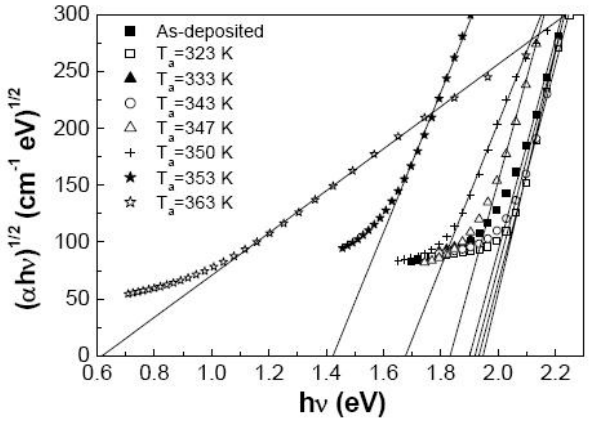

Figure 10: Variation of $(\alpha h\nu)^{1/2}$with photon energy hν for the as-deposited and annealed thin films

where *d* is the film thickness. The values obtained for α are then used to find the optical band gap, E_g[13,15,16]:

$$(\alpha h\nu) = B(h\nu - E_0)^S \quad (5)$$

where b is a constant that depends on the transition probability and the exponent S is an index which determines the types of transition and can take values of 1/2, 3/2, 2, and 3 for allowed direct, forbidden direct, allowed indirect, and forbidden indirect transitions, respectively[14].

The optical absorption measurements for the as-deposited and annealed Se films indicate that the absorption mechanism is due to both the indirect and direct transitions. The optical band gap of the indirect and direct transitions(E_{gi}, E_{gd}) can be obtained from the intercept of the $(\alpha h\nu)^{1/2}$ versus hν plots with the energy axis and, $(\alpha h\nu)^2$ versus, hν respectively, as shown in figures 10 and 11. The dependence of the energy gap on the annealing temperature of amorphous Se films is shown in figure 12.

The reduction of the optical energy gap with annealing temperature has been observed in some chalcogenide films[16,21]. This decease of direct and indirect optical energy gaps with thermal annealing at temperatures higher than glass transition temperature, T_g(figure 13), can be interpreted in terms of inducing crystallization in semiconducting glasses. The results obtained by the XRD, SEM, and AFM studies revealed, as discussed earlier, the absence of any recognizable structure for the as-deposited film, which is typical of the amorphous state. After annealing at temperatures higher thanT_g, the structure

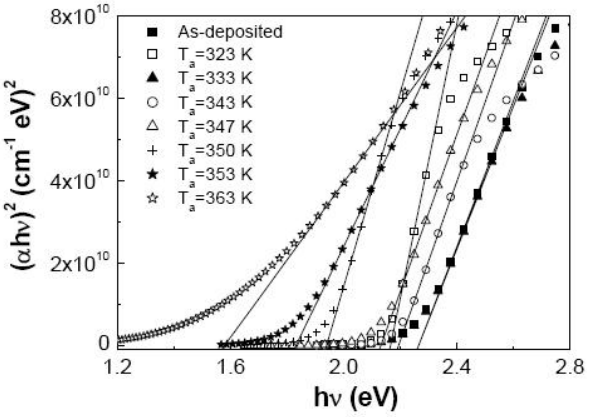

Figure 11: Variation of $(\alpha h\nu)^2$with photon energy hν for the as-deposited and annealed thin films

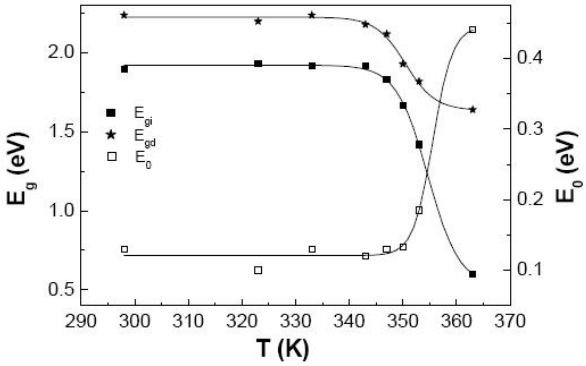

Figure 12: The effect of the annealing temperature on the indirect energy gap, E_{gi}, on the direct energy gap, E_{gd}, and on the width of localized state, E_o

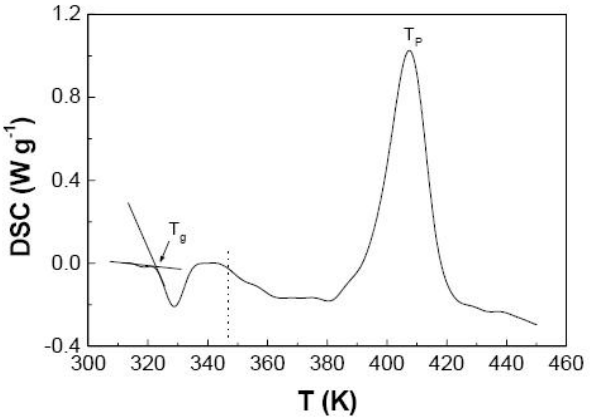

Figure 13: Typical DSC traces at a heating rate of 30 Kmin^{-1} for Se thin films

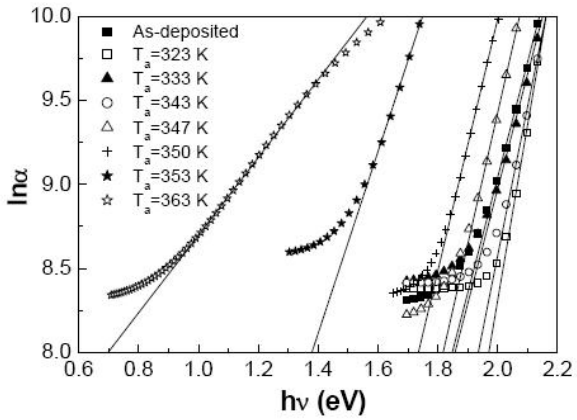

Figure 14: Variation of In α with photon energy hν for the as-deposited and annealed thin films

investigation shows the presence of polycrystalline phases. During annealing at temperatures higher thanT_g, enough vibrational energy is present to break some weaker bonds, thus introducing some translational degree of freedom to the system and resulting

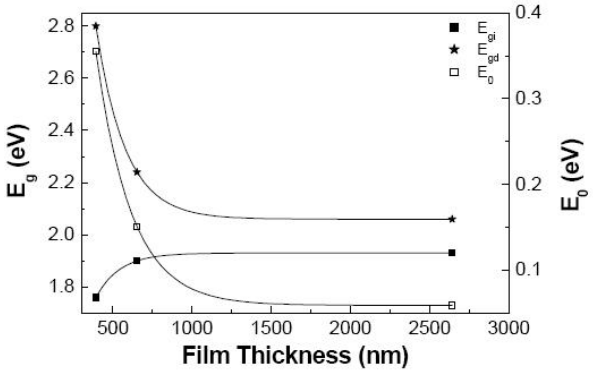

Figure 15: The effect of the film thickness on the indirect energy gap, E_{gi}, on the direct E_{gi} energy gap, E_{gd}, and on the width of localized state, E_o

in an increase in the heat capacity of the system and a decrease in the optical energy gap[16,21].

The absorption coefficients of the optical absorption near the band edge in many amorphous semiconductors show an exponential dependence on photon energy, $h\nu$ and obey Urbach's empirical relation[22]:

$$\alpha = \alpha_0 \exp\left(\frac{h\nu}{E_0}\right) \quad (6)$$

where α_0 is a constant and E_0 is the Urbach energy, which represents the width of the band tails of the localized states in the band gap. The energy E_0 characterizes the slope of the exponential edge region and is almost temperature independent at low temperature. Plots of in a as a function of the photon energy, hν, for Se films at different annealing temperatures are shown in figure 14. The calculated values of E_0 were already shown to be a function of the annealing temperature in figure 12; the value of E_0 for a range of amorphous semiconductors lies between 0.045 and 0.67 eV[23]. As can be seen from figure 12, E_0 is almost constant below 347 K. Since E_0 is generally considered to represent the degree of disorder[24], then increasing the annealing temperature above 347 K leads to an increase in the disorder of the films.

To show if E_{gi},E_{gd} and E_o vary with film thickness, the values of these parameters for as-deposited films were calculated for the three film thicknesses mentioned earlier. The results obtained indicate that the indirect energy gap, E_{gi}, increases on increasing the film thickness, while the direct energy gap, E_{gd}, decreases. Figure 15 shows the obtained values of

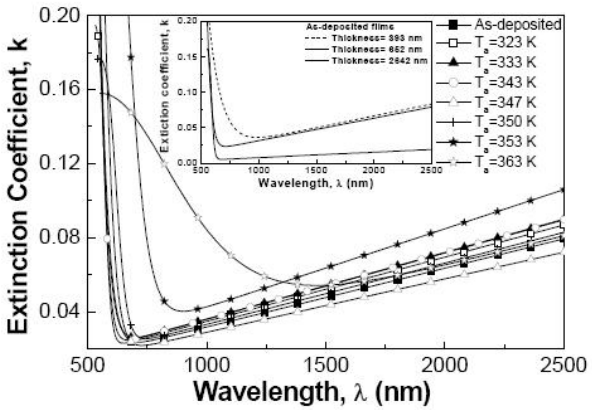

Figure 16: The spectral distribution of the extinction coefficient k(λ) for the Se thin films, both as-deposited and as obtained at different annealing temperatures. The effect of the film thickness on the extinction coefficient is also shown.

E_{gi},E_{gd} and E_o as a function of film thickness.

The values of the extinction coefficient, k, for the investigated Se thin films were calculated from the relation[14].

$$k=\alpha\lambda/4\pi \quad (7)$$

The calculated values of *k* at different annealing temperatures were plotted as a function of wavelength and are shown in figure 16. It was observed that the extinction coefficient tends to increase as the annealing temperature increases. The effect of the film thickness on the extinction coefficient is also shown in figure 16. The results show that the extinction coefficient decreases as the film thickness increases for a certain wavelength.

CONCLUSION

The XRD studies show that the as-deposited films have an amorphous structure. The crystalline phase begins to develop at a transition annealing temperature of 347 K. The surface morphology was investigated by SEM and AFM and showed that the nano-structure grains in the as-deposited film fused together to form larger grains. The optical absorption measurements indicate that the absorption mechanism is due to both indirect and direct transitions. The results obtained showed that the indirect, E_{gi}, and direct, E_{gd}, energy gaps vary with film thickness. Both energies sharply decrease above the annealing temperature of 347 K. The refractive index and the extinction coefficient increase with increasing the annealing temperature; both show a film thickness dependence.

REFERENCES

[1] A.Madan, M.P.Shaw; 'The Physics and Applications of Amorphous Semiconductors', Academic Press, New York, **(1988)**.

[2] T.Katsuyama, S.Satoh, H.Matsumura; J.Appl.Phys., **71**, 4132 **(1992)**.

[3] B.M.Z.Kamaruizaman, C.Juhasz, S.M.Vaezi-Nejad; J.Mater.Sci., **27**, 4316 **(1992)**.

[4] A.Elliott; Nuclear Instruments and Methods in Physics Research., A, **546**, 1 **(2005)**.

[5] J.Holubova, Z.Cemosek, E.Cemoskova, A.Cema; Mater.Lett., **60**, 2429 **(2006)**.

[6] A.A.Joraid; Physica B, **390**, 263 **(2007)**.

[7] N.Tigau; Cryst.Res.Technol., **41**, 474 **(2006)**.

[8] R.Swanepoel; J.Phys.ESci.Instrum., **16**, 1214 **(1983)**.

[9] E.Marquez, J.Ramirez-Malo, P.Villares, R.Jimenez-Garay, P.J.S.Ewen, A.E.Ewen; J.Phys.D Appl.Phys., **25**, 535 **(1992)**.

[10] J.Ramirez-Malo, E.Marquez, P.Villares, R.Jimenez-Garay; Phys.Stat.Sol.(a), **133**, 499 **(1992)**.

[11] J.C.Manifacier, J.Gasiot, J.P.Fillard; J.Phys.ESci. Instrum., **9**, 1002 **(1979)**.

[12] T.S.Moss, G.J.Burrell, B.Ellis; 'Semiconductor Opto-Electronics', Butterworth, London, 19 **(1993)**.

[13] A.S.Soltan, A.A.Abu-Sehly, M.A.Abdel-Rahim; J.Phys.Chem.Solids, **63**, 801 **(2003)**.

[14] S.N.Alamri, A.A.Joraid, S.Y.Al-Raqa; Thin Solid Films, **510**, 265 **(2006)**.

[15] N.Tigau, G.I.Rusua, C.Gheorghies; J.Optoelectron. Adv.Mater., **4**, 943 **(2002)**.

[16] A.El-Korashy, A.Bakry, M.A.Abdel-Rahim, M.Abd El-Sattar; Physica, B, **391**, 266 **(2007)**.

[17] M.M.Hafiz, M.A.Abdel-Rahim, A.A.Abu Sehly; Physica., B, **252**, 207 **(1998)**.

[18] M.A.Abdel-Rahim; J.Phys.Chem.Solids, **60**, 29 **(1999)**.

[19] M.M.Hafiz, O.El-Shazly, N.Kinawy; Appl.Surf.Sci., **171**, 231 **(2001)**.

[20] A.A.Abu-Sehly, A.S.Soltan; Appl.Surf.Sci., **199**, 147 **(2002)**.

[21] A.S.Soltan, M.Abu EL Oyoun, A.A.Abu-Sehly, A.Y.Abdel-Latief; Mater.Chem.Phys., **82**, 101 **(2003)**.

[22] F.Urbach; Phys. Rev., **92**, 1324 **(1953)**.

[23] H.S.Metwally; Vacuum, **62**, 345 **(2001)**.

[24] G.V.Prakash, D.N.Rao, A.K.Bhatnagar; Solid State Commun., **119**, 39 **(2001)**.